Electronic Supplementary Material (ESI) for ChemComm.

Self-supported nickel iron oxide nanospindles with high hydrophilicity for efficient oxygen evolution

Jinlong Liu,[abc‡] Huimin Yuan,[a‡] Zhenyu Wang,[a] Jun Li,[a] Mingyang Yang,[a] Lujie Cao,[a] Guiyu Liu,[b] Dong Qian,[b] and Zhouguang Lu[a]*

[a]Department of Materials Science and Engineering, Southern University of Science and Technology, Shenzhen 518055, China

[b]Hunan Provincial Key Laboratory of Chemical Power Resources, Hunan Provincial Key Laboratory of Efficient and Clean Utilization of Manganese Resources, College of Chemistry and Chemical Engineering, Central South University, Changsha 410083, China

[c]Department of Engineering, University of Cambridge, Cambridge, CB3 0FA, United Kingdom

[‡]J. Liu and H. Yuan contributed equally to this work.

[*]Corresponding Author: Zhouguang Lu, E-mail address: luzg@sustech.edu.cn

Experimental section

Preparation of $NiFe_2O_4$@FNF: $NiFe_2O_4$ nanospindle arrays were grown in situ on FNF (thickness 1 mm, YiYang Foam Metal New Material Co., Ltd) through a facile hydrothermal method. According to previous report,[1,2] the in-situ growth can be explained by a dissolution-precipitation mechanism. Specifically, the HCl first corrodes the surface of $FeNi_3$ foam to Fe and Ni ions. Once the HCl is consumed completely, the generated mixed metal ions further deposit on the $FeNi_3$ substrate to form $NiFe_2O_4$ nanospindle arrays. Typically, a piece of FNF (1 cm × 4 cm) was cleaned in 3 M HCl solution (Sigma-Aldrich, ACS reagent, 37%) and ethanol (Sigma-Aldrich, ≥99.8%) under sonication, and then rinsed with ultra-pure water for use. To prepare the hydrothermal solution, concentrated HCl was diluted with ultra-pure water until the pH of the solution was 2.5, which was measured by a pH meter (Mettler Toledo EL20-Kit Benchtop Education). 40 mL of as-prepared HCl solution was added into a 50 mL Teflon-lined stainless steel autoclave, followed by immersing the cleaned FNF into the acid solution. The autoclave was sealed and kept in a pre-heated oven at 180 °C for 6 h. After natural cooling, the product was collected and underwent ultrasonic treatment for 30 s to remove loosely attached particles. Afterwards, the product was rinsed by water and ethanol for several times, and further dried in a vacuum oven at 60 °C overnight.

Preparation of $Ni(OH)_2$/NF: $Ni(OH)_2$ nanoplate arrays supported on NF (thickness 1 mm, YiYang Foam Metal New Material Co., Ltd) were synthesized for comparison by the same procedures as for the preparation of $NiFe_2O_4$@FNF, except that the FNF was replaced with NF.

Preparation of IrO_2/NF: Commercial IrO_2 (Sigma-Aldrich, 99.9% trace metals basis) catalyst as benchmark OER electrocatalyst was loaded on NF by the same approach in previous report.[3]

Samples for hydrophilicity measurements: To evaluate and compare the hydrophilicity of $NiFe_2O_4$@FNF and the control groups, $FeNi_3$ foam and Ni foam were pressed into flat plates by a roll squeezer and underwent the same hydrothermal treatment as the preparation of $NiFe_2O_4$@FNF and $Ni(OH)_2$@NF to obtain $NiFe_2O_4$@pFNF and $Ni(OH)_2$@pNF, respectively.

Material Characterizations

SEM images were collected on a Quanta 450 field-emission scanning electron microscope. TEM, SAED and HRTEM characterizations were carried out with a Tecnai G^2 F30 transmission electron microscope. XRD patterns were recorded using a Japan Rigaku MiniFlex X-ray diffractometer with graphite monochromatized Cu Kα radiation (λ = 1.540598 Å). XPS spectra were acquired by an ESCALab250 XPS spectrometer.

Electrochemical Measurements

The electrochemical properties of all samples were investigated on a 760D electrochemical workstation (CH Instruments, Inc., USA) using a standard three-electrode glass cell (Pine Research Instruments, USA), in which $NiFe_2O_4$@FNF, IrO_2/NF, $Ni(OH)_2$/NF, pristine FNF and NF were used as working electrode, a carbon rod as the counter electrode, an Ag/AgCl (4 M KCl) electrode as the reference electrode, and the electrolyte was 1.0 M KOH (Sigma-Aldrich, reagent grade, 90%) aqueous solution. Prior to the electrochemical measurements, the electrolyte was purged with O_2 for 30 min to reach O_2/H_2O equilibrium at 1.23 V vs. RHE. After several CV cycling at a scan rate of 10 mV s^{-1} to get stabilized signals, the LSV curves were collected at a scan rate of 1 mV s^{-1} to evaluate the OER polarization. Chronoamperometry was adopted to study the durability in prolonged operation. CV curves in a potential window of 0.85−0.90 V vs. RHE at different

scan rates from 10 to 50 mV s^{-1} were recorded to calculate the C_{dl}. Electrochemical impedance spectroscopy (EIS) was measured at 1.50 V vs. RHE in the frequency range from 0.1 Hz to 100 kHz with an amplitude of 5 mV. All the potentials vs. Ag/AgCl were converted to a RHE scale according to the Nernst equation: E(RHE) = E(Ag/AgCl) + 0.205 + 0.059 × pH, and iR correction was conducted using the solution resistance (R_s) estimated from the EIS simulation result. The apparent current density was normalized to the geometrical area of working electrode. All electrochemical measurements were performed at room temperature.

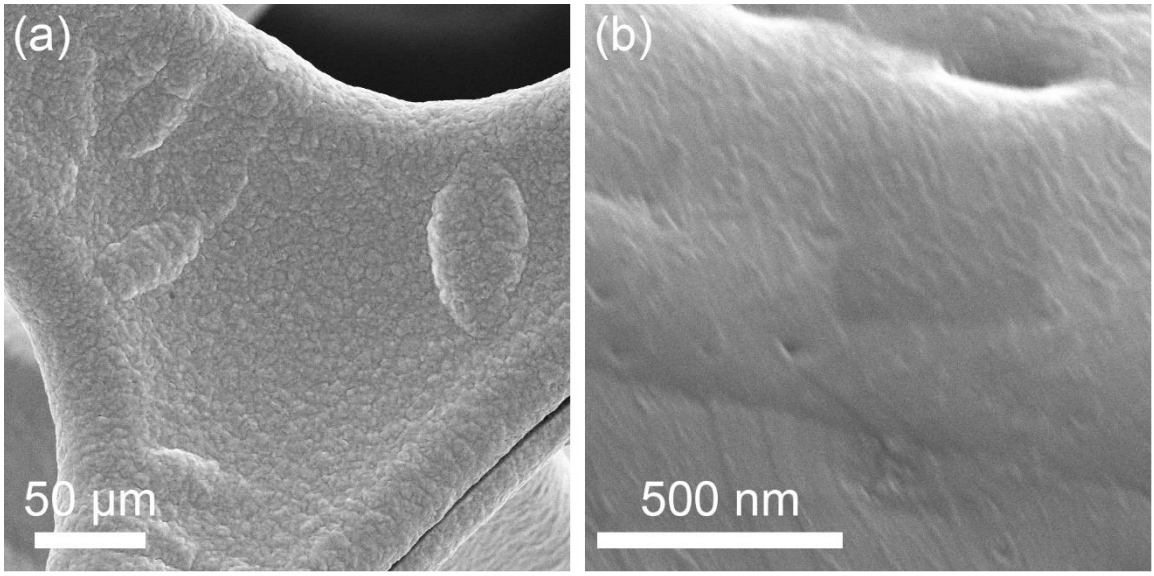

Fig. S1 SEM images of pristine $FeNi_3$ foam.

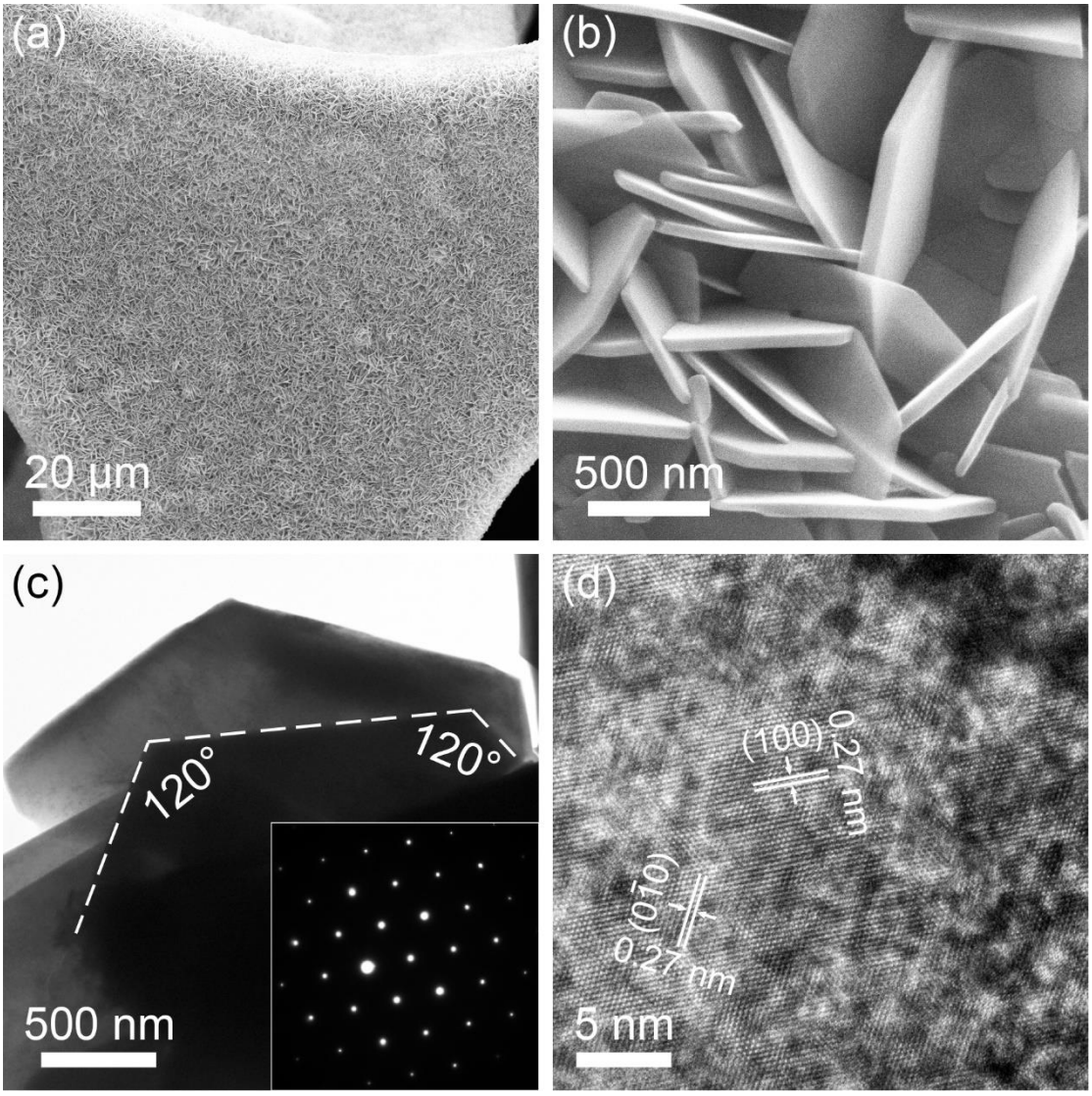

Fig. S2 (a,b) SEM images of $Ni(OH)_2$@NF. (c) TEM, and d) HRTEM images of corresponding $Ni(OH)_2$ nanoplates. The inset in panel (c) shows the SAED pattern of $Ni(OH)_2$ nanoplates.

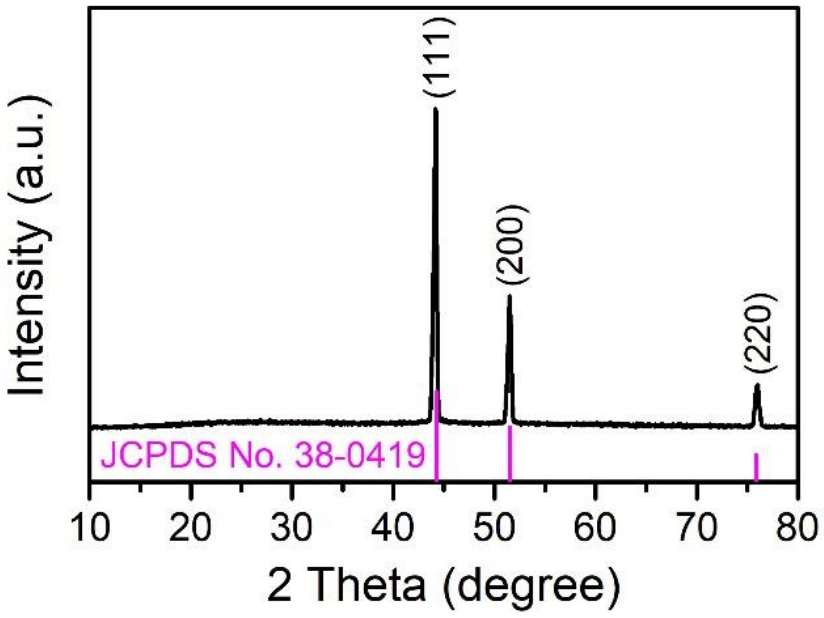

Fig. S3 XRD pattern of $FeNi_3$ alloy foam with standard XRD pattern of $FeNi_3$ for reference.

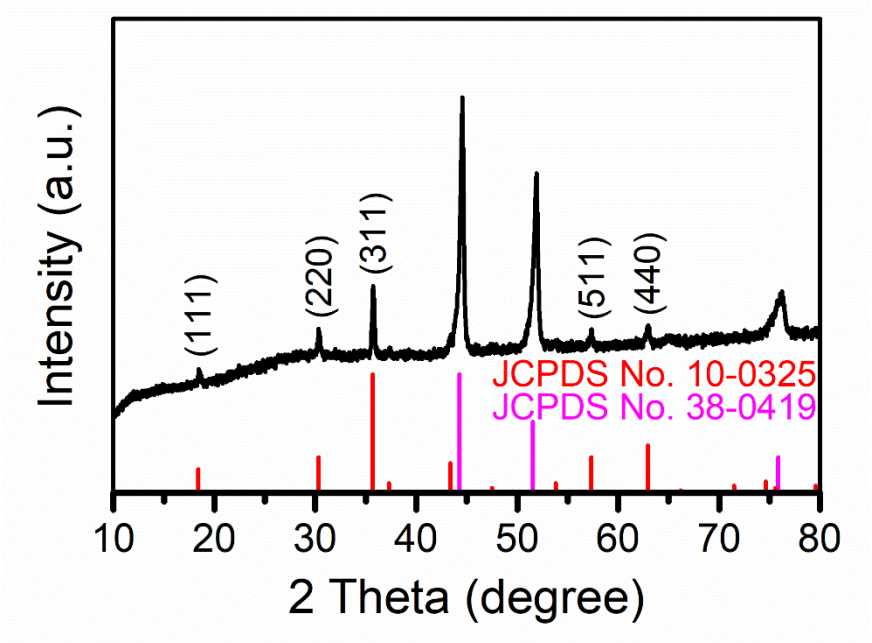

Fig. S4 XRD pattern of $NiFe_2O_4$@FNF with standard XRD patterns of $NiFe_2O_4$ and $FeNi_3$ for reference.

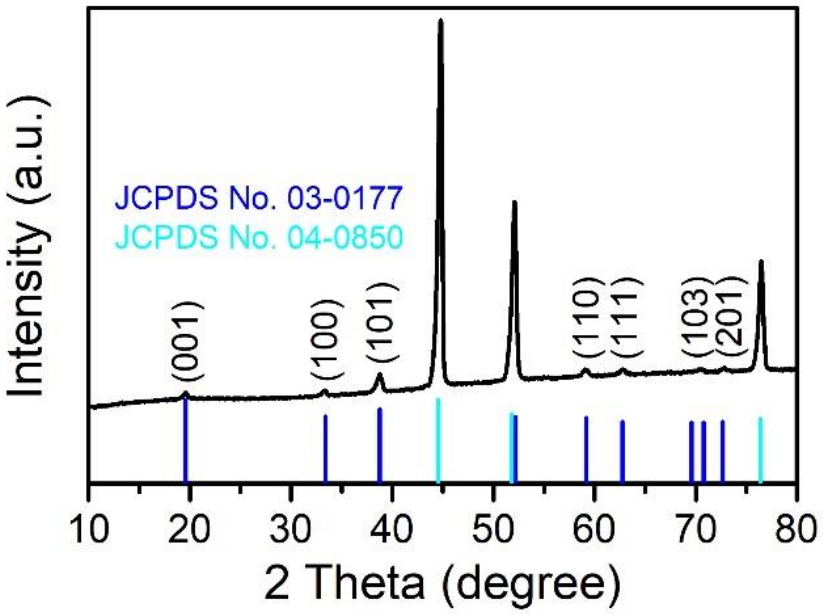

Fig. S5 XRD pattern of $Ni(OH)_2$@NF with standard XRD patterns of $Ni(OH)_2$ and Ni for reference.

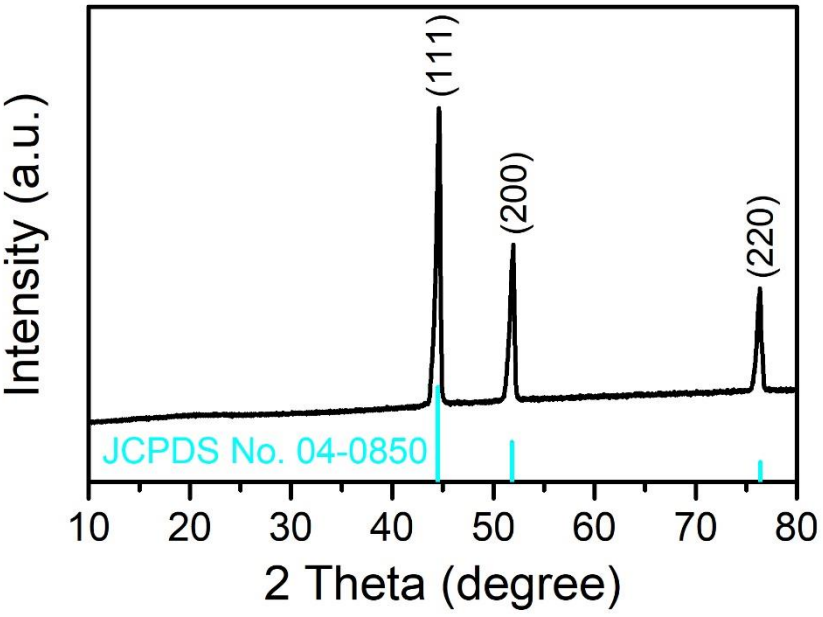

Fig. S6 XRD pattern of Ni foam with standard XRD pattern of Ni for reference.

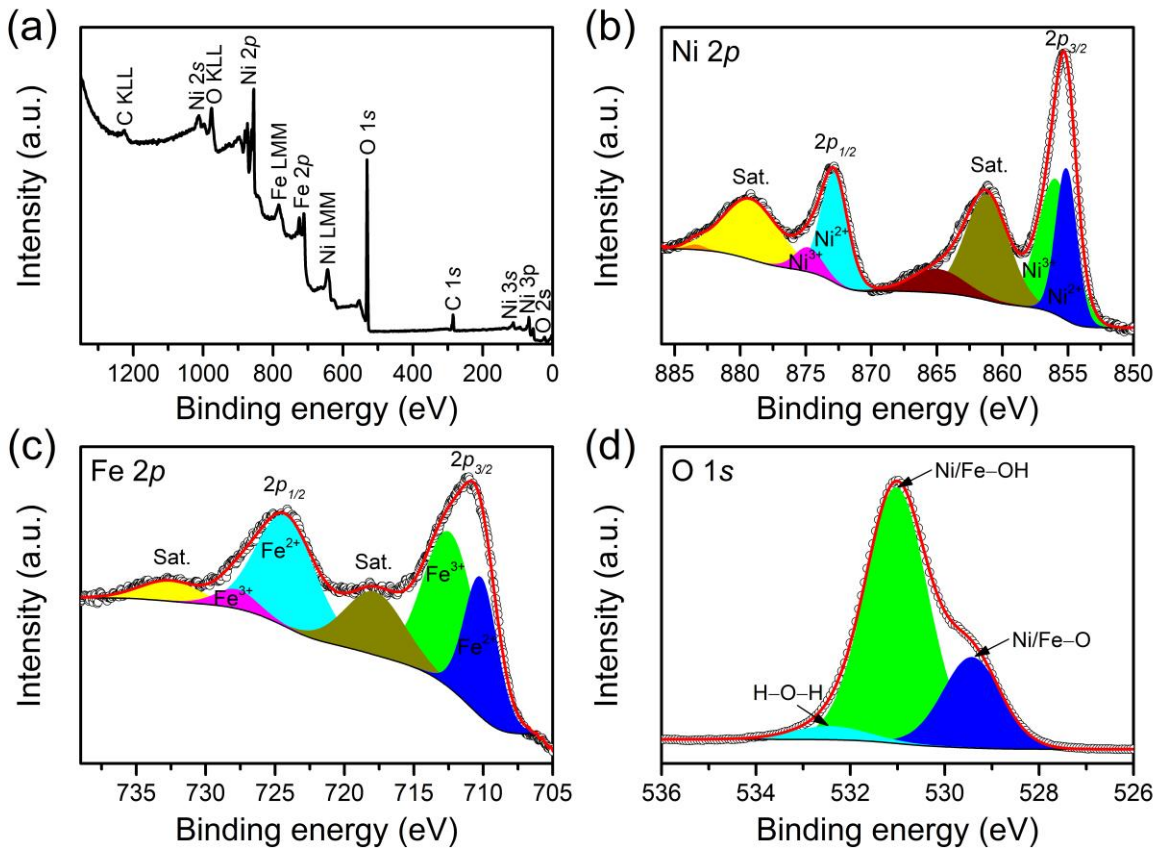

Fig. S7 (a) Survey XPS spectrum, (b) Ni 2p, (c) Fe 2p, and (d) O 1s high-resolution XPS spectra of $NiFe_2O_4$@FNF.

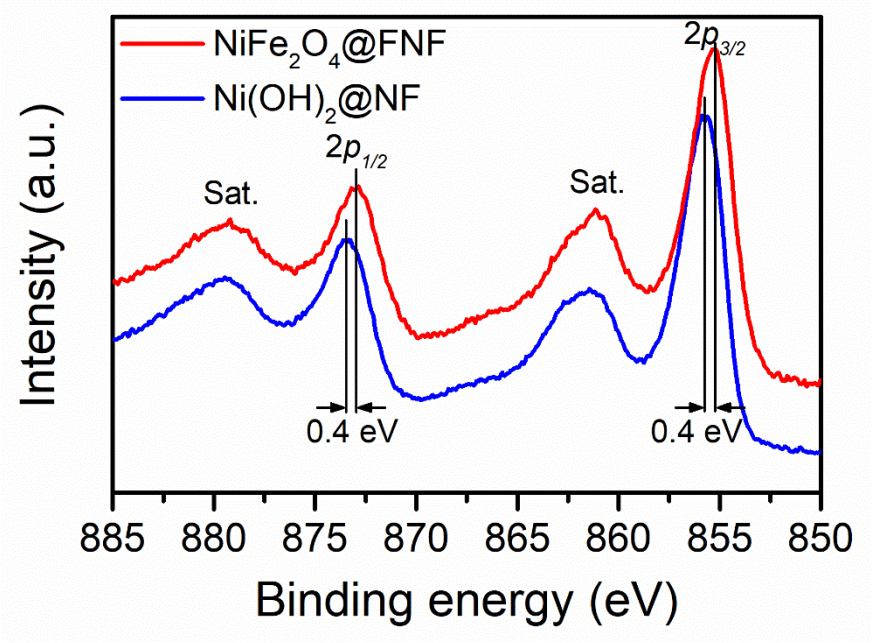

Fig. S8 Comparison of Ni 2p high-resolution XPS spectra for $NiFe_2O_4$@FNF and $Ni(OH)_2$@NF.

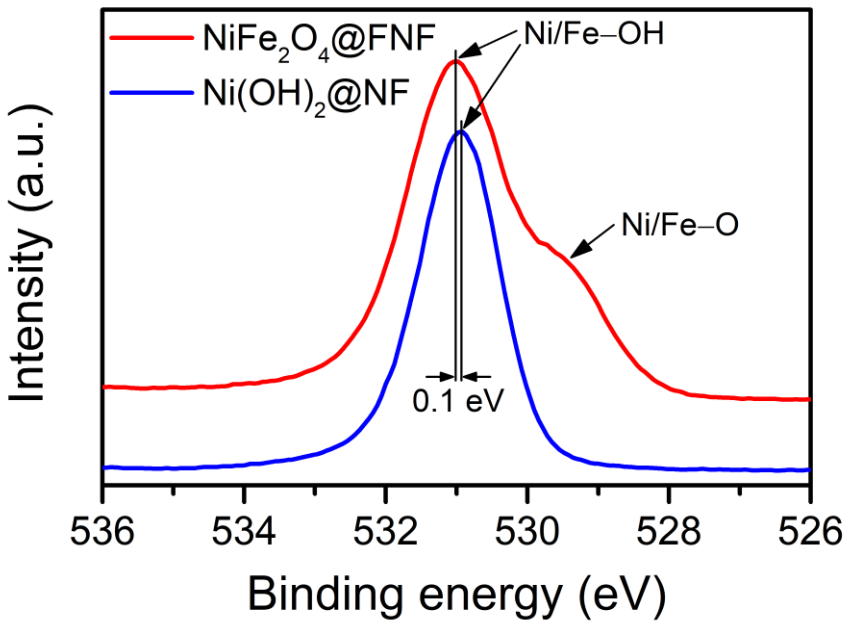

Fig. S9 Comparison of O 1s high-resolution XPS spectra for $NiFe_2O_4$@FNF and $Ni(OH)_2$@NF.

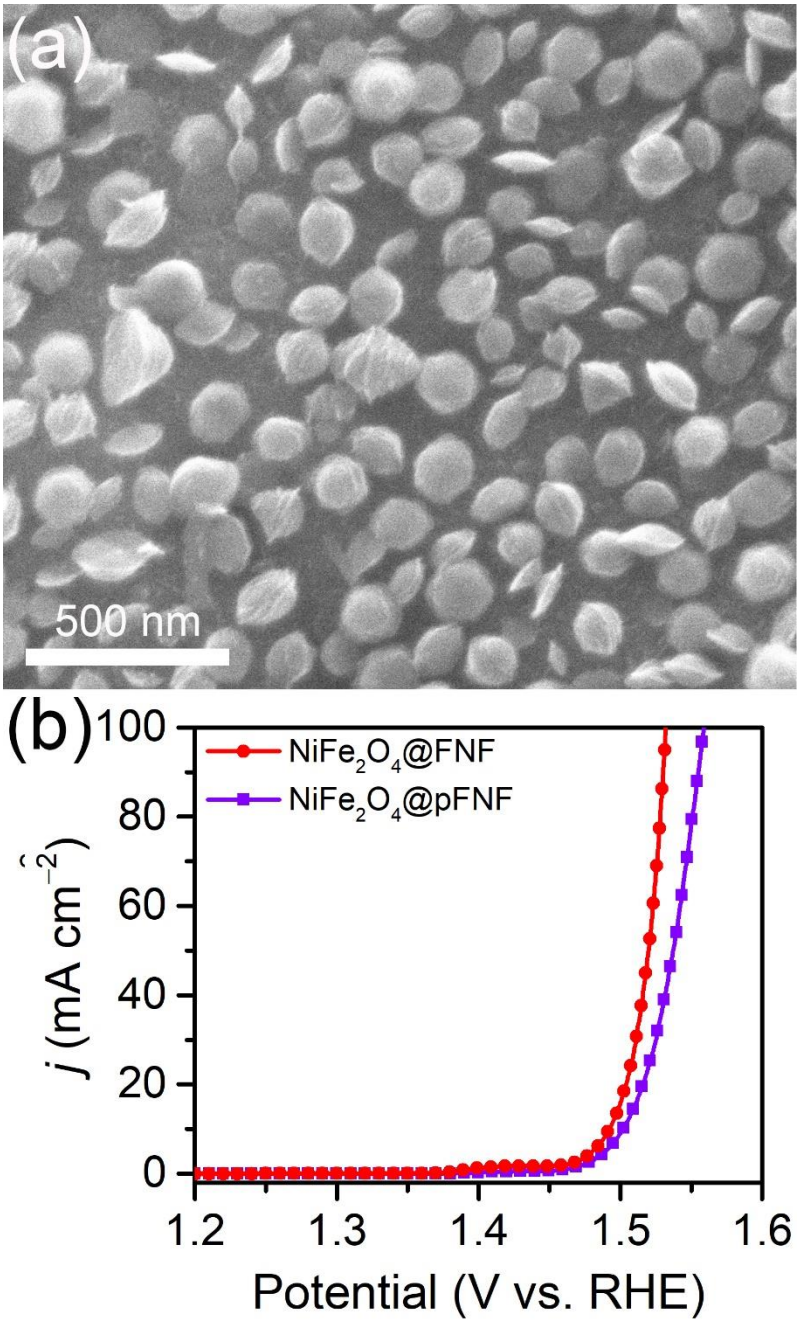

Fig. S10 (a) SEM image of $NiFe_2O_4$@pFNF. (b) OER polarization curves of $NiFe_2O_4$@FNF and $NiFe_2O_4$@pFNF in 1.0 M KOH at a scan rate of 1 mV s^{-1}.

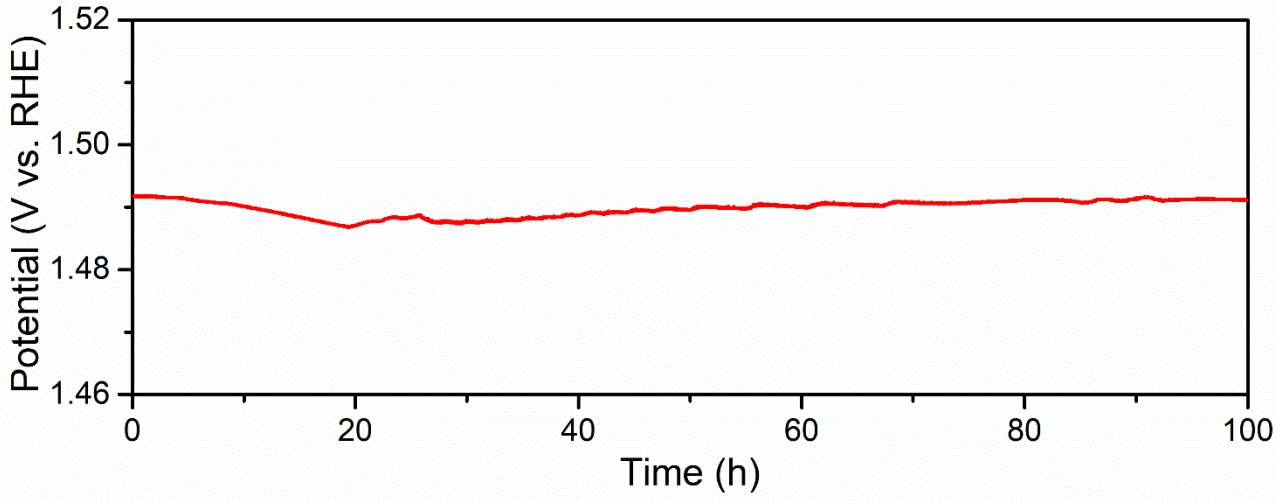

Fig. S11 Chronopotentiometric curve of $NiFe_2O_4$@FNF in 1.0 M KOH to deliver 10 mA cm^{-2} for 100 h.

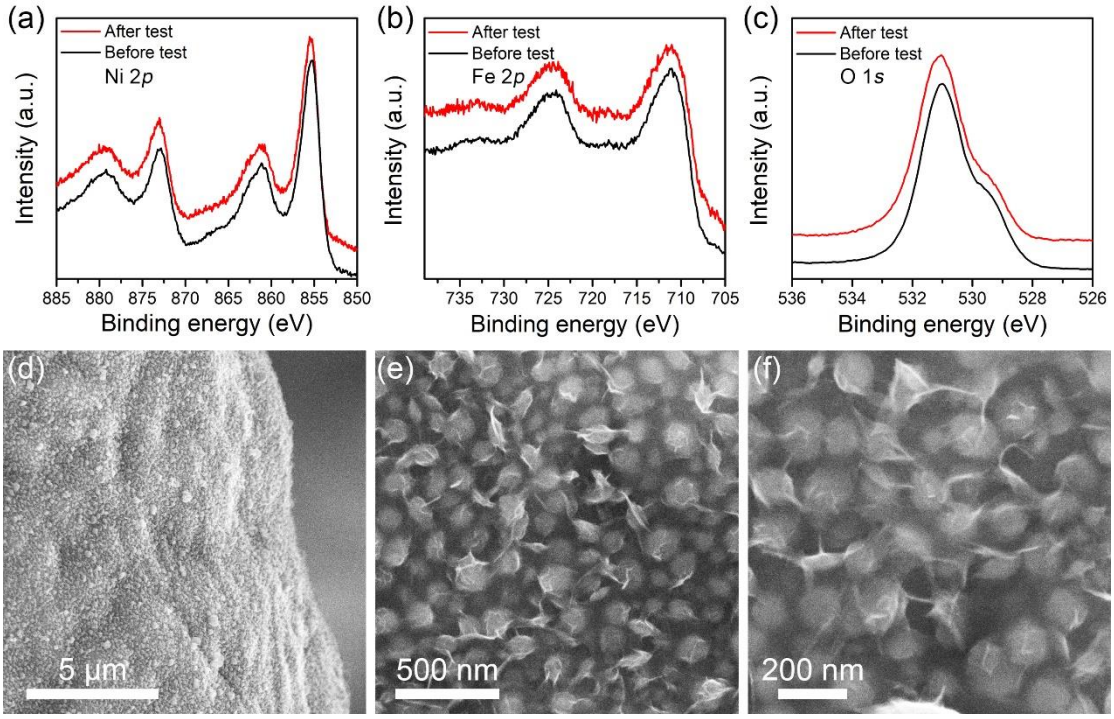

Fig. S12 (a) Ni 2p, (b) Fe 2p, and (c) O 1s high-resolution XPS spectra of $NiFe_2O_4$@FNF before and after OER stability test. (d–f) SEM image s of $NiFe_2O_4$@FNF after OER stability test.

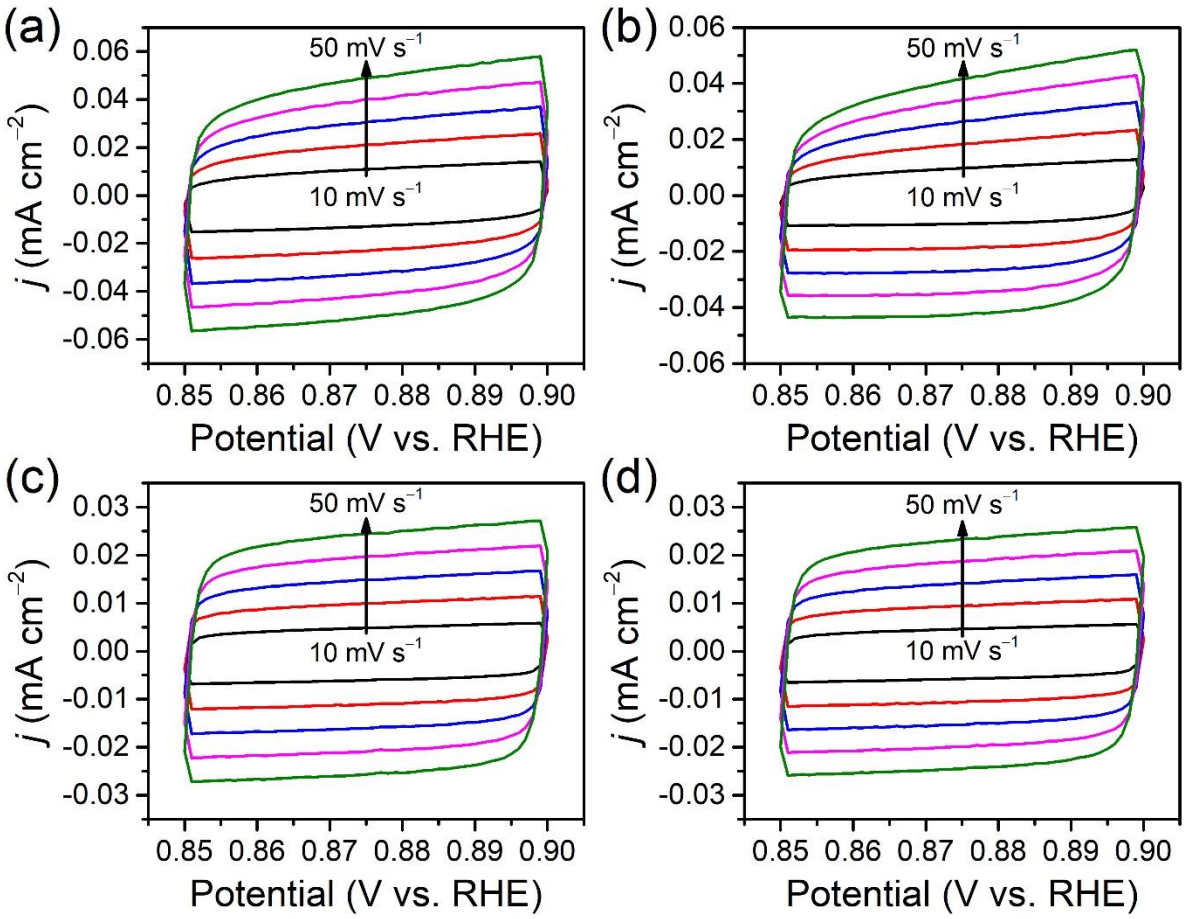

Fig. S13 CV curves of (a) $NiFe_2O_4$@FNF, (b) $Ni(OH)_2$@NF, (c) FNF, and (d) NF in a potential window of 0.85–0.90 V vs. RHE without faradaic processes at scan rates from 10 to 50 mV s^{-1}.

Table S1. Comparison of $NiFe_2O_4$ based OER electrocatalysts in alkaline electrolyte.

Catalysts	Electrode	Electrolyte	OER η_{10} (mV)	OER Tafel slop (mV dec^{-1})	Ref.
$NiFe_2O_4$@FNF	FeNi foam	1.0 M KOH	262	39.5	This work
FeNi/$NiFe_2O_4$@NC-800	Glassy carbon	1.0 M KOH	316	60	4
$NiFe_2O_4$	Carbon paper	1.0 M KOH	381	46.4	5
AT $NiFe_2O_4$ QDs	Glassy carbon	1.0 M KOH	262	37	6
$NiFe_2O_4$ nanorods	Glassy carbon	1.0 M KOH	342	44	7
$NiFe_2O_4$ nanosheets	Glassy carbon	1.0 M NaOH	460	80	8
S-$NiFe_2O_4$/Ni_3Fe/NW	Ni wire	1.0 M KOH	240	35	9
$NiFe_2O_4$/NF	Ni foam	1.0 M KOH	293	98	10
NiO-$NiFe_2O_4$/rGO	Glassy carbon	1.0 M KOH	296	42.8	11
Nickel-iron oxide/carbon	Glassy carbon	1.0 M KOH	310	42	12
S-$NiFe_2O_4$/NF	Ni foam	1.0 M KOH	267	36.7	13

Table S2. Comparison of recently reported earth-abundant electrocatalysts for the OER in alkaline electrolyte.

Catalysts	Electrode	Electrolyte	OER η_{10} (mV)	OER Tafel slop (mV dec^{-1})	Ref.
$NiFe_2O_4$@FNF	FeNi foam	1.0 M KOH	262	39.5	This work
NiCo nanopyramid	Cu foil	1.0 M NaOH	307	63	14
$Fe_{0.4}Co_{0.6}$ composite film	Carbon fiber paper	1.0 M KOH	283	34	15
Fe-Ni nanoparticle	Glassy carbon	1.0 M NaOH	311	-	16
NiFe@g-C_3N_4/CNT	Glassy carbon	1.0 M KOH	326	67	17
De-Li$Co_{0.33}Ni_{0.33}Fe_{0.33}O_2$	Carbon fiber paper	0.1 M KOH	295	35	18
L-Co_3O_4	Carbon fiber	1.0 M KOH	294	74	19
$Ni_xCo_yO_4$ (x/y = 1/4)	Glassy carbon	1.0 M KOH	336	36	20
$PrBa_{0.5}Sr_{0.5}Co_{1.5}Fe_{0.5}O_{5+\delta}$	Glassy carbon	0.1 M KOH	358	52	21
Iron fluoride-oxide nanoporous film	Fe foil	1.0 M KOH	260	45	22
Exfoliated NiFe LDH nanosheet	Glassy carbon	1.0 M KOH	300	40	23
α-$Co(OH)_2$-Cl	Glassy carbon	1.0 M KOH	320	53	24
$Co(OH)_2$@NCNT@NF	Ni foam	1.0 M KOH	270	72	25
CoN-1 min	Ni foam	1.0 M KOH	290	70	26
Co_4N porous nanowire	Carbon cloth	1.0 M KOH	257	44	27
Mn_3N_2	Nickel foam	1.0 M KOH	270	101	28
CoP@RGO	Glassy carbon	1.0 M KOH	280	75	29
$Fe_{1.1}Mn_{0.9}P$ nanorods	Glassy carbon	1.0 M KOH	440	39	30
$Ni_{0.65}Fe_{0.35}P$	Glassy carbon	1.0 M KOH	270	60	31

Table S3. Electrochemical analysis of $NiFe_2O_4$@FNF, $Ni(OH)_2$@NF, FNF and NF.

Sample	Double-layer capacitance (C_{dl}, μF cm^{-2})	Roughness factor (R_f)[a]	*j* @ 1.50 V vs. RHE (mA cm^{-2})	$j_{specific}$ @ 1.50 V vs. RHE (mA cm^{-2})[b]
$NiFe_2O_4$@FNF	946.95	15.78	15.93	1.009
$Ni(OH)_2$@NF	799.77	13.33	1.56	0.117
FNF	490.46	8.17	0.309	0.038
NF	467.8	7.80	0.208	0.027

[a]According to previous report,[32] the C_{dl} of an ideal flat electrode is ~60 μF cm^{-2}. R_f is therefore calculated using $R_f = \frac{C_{dl}}{60} \times 1000$.

[b]$j_{specific}$ is calculated using $j_{specific} = \frac{j}{R_f}$, where *j* is the apparent OER current density.

Reference

1 J. Tian, Z. Xing, Q. Chu, Q. Liu, A. M. Asiri, A. H. Qusti, A. O. Al-Youbi and X. Sun, *CrystEngComm*, 2013, **15**, 8300−8305.

2 J. Liu, Y. Zheng, Z. Wang, Z. Lu, A. Vasileff and S.-Z. Qiao, *Chem. Commun.*, 2018, **54**, 463−466.

3 J. Liu, Y. Zheng, Y. Jiao, Z. Wang, Z. Lu, A. Vasileff and S.-Z. Qiao, *Small*, 2018, **14**, 1704073.

4 Y. Ma, X. Dai, M. Liu, J. Yong, H. Qiao, A. Jin, Z. Li, X. Huang, H. Wang and X. Zhang, *ACS Appl. Mater. Interfaces*, 2016, **8**, 34396−34404.

5 V. Maruthapandian, M. Mathankumar, V. Saraswathy, B. Subramanian and S. Muralidharan, *ACS Appl. Mater. Interfaces*, 2017, **9**, 13132−13141.

6 H. Yang, Y. Liu, S. Luo, Z. Zhao, X. Wang, Y. Luo, Z. Wang, J. Jin and J. Ma, *ACS Catal.*, 2017, **7**, 5557−5567.

7 G. Liu, K. Wang, X. Gao, D. He and J. Li, *Electrochim. Acta*, 2016, **211**, 871−878.

8 C. Mahala, M. D. Sharma and M. Basu, *Electrochim. Acta*, 2018, **273**, 462−473.

9 M. Y. Gao, J. R. Zeng, Q. B. Zhang, C. Yang, X. T. Li, Y. X. Hua and C. Y. Xu, *J. Mater. Chem. A*, 2018, **6**, 1551−1560.

10 Z. Fang, Z. Hao, Q. Dong and Y. Cui, *J. Nanopart. Res.*, 2018, **20**, 106.

11 G. Zhang, Y. Li, Y. Zhou and F. Yang, *ChemElectroChem*, 2016, **3**, 1927−1936.

12 H. Chen, X. Huang, L.-J. Zhou, G.-D. Li, M. Fan and X. Zou, *ChemCatChem*, 2016, **8**, 992−1000.

13 J. Liu, D. Zhu, T. Ling, A. Vasileff and S.-Z. Qiao, *Nano Energy*, 2017, **40**, 264−273.

14 R. K. Vishnu Prataap and S. Mohan, *Chem. Commun.*, 2017, **53**, 3365−3368.

15 W. Liu, K. Du, L. Liu, J. Zhang, Z. Zhu, Y. Shao and M. Li, *Nano Energy*, 2017, **38**, 576−584.

16 S. L. Candelaria, N. M. Bedford, T. J. Woehl, N. S. Rentz, A. R. Showalter, S. Pylypenko, B. A. Bunker, S. Lee, B. Reinhart, Y. Ren, S. P. Ertem, E. B. Coughlin, N. A. Sather, J. L. Horan, A. M. Herring and L. F. Greenlee, *ACS Catal.*, 2017, **7**, 365−379.

17 D. Liu, S. Ding, C. Wu, W. Gan, C. Wang, D. Cao, Z. u. Rehman, Y. Sang, S. Chen, X. Zheng, Y. Wang, B. Ge and L. Song, *J. Mater. Chem. A*, 2018, **6**, 6840−6846.

18 Z. Lu, H. Wang, D. Kong, K. Yan, P.-C. Hsu, G. Zheng, H. Yao, Z. Liang, X. Sun and Y. Cui, *Nat. Commun.*, 2014, **5**, 4345.

19 Y. Zhou, C.-K. Dong, L. L. Han, J. Yang and X.-W. Du, *ACS Catal.*, 2016, **6**, 6699−6703.

20 X. Deng, S. Öztürk, C. Weidenthaler and H. Tüysüz, *ACS Appl. Mater. Interfaces*, 2017, **9**, 21225−21233.

21 B. Zhao, L. Zhang, D. Zhen, S. Yoo, Y. Ding, D. Chen, Y. Chen, Q. Zhang, B. Doyle, X. Xiong and M. Liu, *Nat. Commun.*, 2017, **8**, 14586.

22 X. Fan, Y. Liu, S. Chen, J. Shi, J. Wang, A. Fan, W. Zan, S. Li, W. A. Goddard and X.-M. Zhang, *Nat. Commun.*, 2018, **9**, 1809.

23 F. Song and X. Hu, *Nat. Commun.*, 2014, **5**, 4477.

24 P. F. Liu, S. Yang, L. R. Zheng, B. Zhang and H. G. Yang, *J. Mater. Chem. A*, 2016, **4**, 9578−9584.

25 P. Guo, J. Wu, X.-B. Li, J. Luo, W.-M. Lau, H. Liu, X.-L. Sun and L.-M. Liu, *Nano Energy*, 2018, **47**, 96−104.

26 Y. Zhang, B. Ouyang, J. Xu, G. Jia, S. Chen, R. S. Rawat and H. J. Fan, *Angew. Chem. Int. Ed.*, 2016, **55**, 8670−8674.

27 P. Chen, K. Xu, Z. Fang, Y. Tong, J. Wu, X. Lu, X. Peng, H. Ding, C. Wu and Y. Xie, *Angew. Chem. Int. Ed.*, 2015, **54**, 14710−14714.

28 C. Walter, P. W. Menezes, S. Orthmann, J. Schuch, P. Connor, B. Kaiser, M. Lerch and M. Driess, *Angew. Chem. Int. Ed.*, 2018, **57**, 698−702.

29 G. Zhang, G. Wang, Y. Liu, H. Liu, J. Qu and J. Li, *J. Am. Chem. Soc.*, 2016, **138**, 14686−14693.

30 D. Li, H. Baydoun, B. Kulikowski and S. L. Brock, *Chem. Mater.*, 2017, **29**, 3048−3054.

31 Z. Liu, G. Zhang, K. Zhang, H. Liu and J. Qu, *ACS Sustainable Chem. Eng.*, 2018, **6**, 7206−7211.

32 S. Levine and A. L. Smith, *Discuss. Faraday Soc.*, 1971, **52**, 290−301.